Computer simulations of fragmentation in nuclear reactions: A semiclassical model

Glenn E. Beauvais, David H. Boal, and John C. K. Wong

Department of Physics, Simon Fraser University, Burnaby, British Columbia, Canada V5A 1S6

A semiclassical model is used to perform numerical simulations of the production of nuclear fragments in both proton- and heavy-ion-induced reactions. The Pauli principle is incorporated by means of a collision term, as it is in the Vlasov-Uehling-Uhlenbeck equation. The model goes beyond the Vlasov-Uehling-Uhlenbeck equation by propagating on an event-by-event basis the phase space fluctuations which develop during a nuclear reaction. Both the Coulomb and isospin-dependent interaction terms are included. For proton-induced reactions at intermediate energies, fragment production is found to be a fairly infrequent process, as is observed experimentally. Heavy-ion reactions show much greater fragment yields. For these latter reactions, we have compiled sufficiently many events so as to be able to compare the predicted fragment yields with experiment. The isotopic distribution of products, as well as their distribution in momentum space, are also examined. The events are used to generate a two-particle correlation function. Analysis of the energy-summed two-proton correlations indicates a large source region. The coordinate and phase space reaction trajectories are followed for a central collision, and preliminary evidence is found in the simulations for the onset of mechanical instability.

I. INTRODUCTION

Computer simulations have been used for some time in the investigation of intermediate energy nuclear reactions. (For a sampling of previous work, see Refs. 1—9 and references therein). Recently, the question of fragment production in these reactions was addressed by propagating on an event-by-event basis the phase space fluctuations which develop from collision processes during a reaction. Depending on the conditions, these fluctuations may be strong enough to ultimately manifest themselves as nuclear fragments. This idea has been implemented in several methods: Two-dimensional time-dependent Hartree Fock (2-D TDHF),[10] molecular dynamics,[11] and variations of the Vlasov equation.[12,13] Much of the work so far has concentrated on the properties of single nuclei at various compression/temperature combinations. Heavy ion reactions were first investigated using this technique in Ref. 12 by using a cascade model (with NN collisions but no mean field) to represent the interpenetration phase of the reaction, the results from which were then propagated with a mean field (but no NN collisions).

What we wish to present here is a simulation involving both NN collisions and a mean field. The ingredients of the simulation are similar to the methods used to solve the Vlasov-Uehling-Uhlenbeck (VUU) equation which has been used before[6–9] to successfully describe, among other things, such observables as the nucleon energy spectrum in a heavy ion reaction. The VUU approach has not generally been applied to fragment formation because fluctuations and correlations are averaged out. Our philosophy here will be different: We start with the classical A-body problem including correlations, but include a new way of handling the Pauli blocking problem, which allows propagation on a single event basis and hence preserves the fluctuations. This allows us to include Fermi motion

and construct more realistic nuclei than what one can classically. However, the model is still not a full quantum model: The uncertainty principle is included only to the extent that a nucleon is spread out in phase space with a Gaussian distribution; there is no variable de Broglie wavelength. We refer to the technique as a semiclassical equations of motion (SCEOM) model.

The NN interaction includes not only the bulk potential term used in previous VUU simulations, but also Coulomb and isospin-dependent terms. These latter terms affect product mass distributions and energy spectra and allow a more realistic comparison with experimental data. The calculational method is outlined in Sec. II. In Sec. III, the results of tests of the initialization procedure for a single ideal nucleus are given. The technique is applied to proton-induced reactions in that section as well, and to heavy ion reactions in Sec. IV.

In these calculations, our approach will be to assume a particular parametrization of the nuclear mean field. The mean field then determines the static properties, such as rms radius, density distribution, binding energy, etc., of a nucleus with a given Z and N. Hence, a search must be made over the parameters in the initialization procedure to ensure that the predicted properties for a given nucleus actually are close to what is experimentally known. With the conventional functional form chosen, we do not obtain perfect agreement with the known properties of a given nucleus, although the disagreements are generally small. In turn, this allows us to make at least qualitative comparisons with reaction data, where statistics permit. Such comparisons are included in Sec. IV.

In Sec. V, we move beyond the predictions of inclusive properties of a reaction and obtain a two-particle correlation function at small momentum difference (nuclear interferometry). Direct comparison with data is not possible because the mean field does not reproduce the low en-

ergy NN phase shifts. However, we can make an internal comparison by independently using the mean field to generate a correlation function assuming that the particles come from a source with a Gaussian distribution in space.

Of course, the purpose for performing computer simulations is not simply to reproduce data. Among other things, the simulations allow us to examine the space-time evolution of the reaction, subject to the model dependence of the simulation. In Sec. VI, the temporal evolution of the trajectories of reaction products in coordinate space and phase space is examined. While no discontinuities such as might be expected from a liquid-gas phase transition are observed in these simulations, nevertheless, indirect information is obtainable about the breakup in the mechanical instability region. Lastly, our conclusions are summarized in Sec. VII.

II. METHODOLOGY

The most difficult aspect of the simulation is the initialization of the target and projectile nuclei in a configuration which approximates the real ground state. In a completely classical system[4–6] the ground state is usually crystalline and is relatively straightforward to construct. The semiclassical nucleus described here is in some sense a metastable excited state, in that the collision term mocks up the Pauli principle and helps prevent the nucleus from collapsing to the true ground state. Such nuclei will not be infinitely stable: The pressure of local fluctuations in phase space means that occasionally a nucleon will scatter to a region of phase space where it is potentially unbound. In most cases, subsequent scatterings will lower the energy of such a nucleon back down and prevent emission. Hence, "accidental" nucleon evaporation will take place, but on the long time frame of hundreds of fm/c, much longer than the collision time frame for intermediate and high energy reactions. Still, this is a characteristic of this approach which limits its ability to describe very long time scale processes, or ones in which only a few MeV per nucleon have been deposited in the reaction region. for the problems which will be examined here, the restriction is unimportant.

A. Initialization

The numerical simulation of one-body distribution functions, such as are described by the Boltzmann, Vlasov, or other equations, often involve taking a random sample of the ground state phase space distribution. This ensemble of test particles is then propagated in time according to the dynamics which govern the equation being simulated. Where accurate knowledge of the distribution is required for evaluating a quantity during the simulation (e.g., evaluation of phase space for determining Pauli blocking) many test particles can be used in a given ensemble, or an average can be made over many ensembles run in parallel.

Such a Monte Carlo initialization is not appropriate here, however, because too much excitation energy is introduced into the system by the fluctuations in density. For example, because the mean field term (see below) associated with the nuclear force corresponds to a max-

imum in the binding energy at nuclear matter density ($\rho_0 = 0.17$ fm^{-3} here), density fluctuations around ρ_0 will correspond to regions of increased energy. Similarly, large increases in potential energy can arise from protons being placed too close to each other by the Monte Carlo procedure. Here, we use a lattice initialization in coordinate space to minimize the effects of fluctuations on the potential energy. Even though the lattice has a potential energy of its own, it can be easily manipulated by means of varying the lattice spacing. The initialization procedure is as follows:

1. A body-centered cubic lattice with edge length l (corresponding to a density $2/l^3$) is used. For various mass numbers, a search is made to find lattices which are as "spherical" as possible. The most stable configurations over the mass range 27–197 were found for $l = 2.12$ fm. Although this corresponds to an initial central density for heavy nuclei which is somewhat greater than nuclear matter density, the nuclei relax away from this value after a short period of time.

2. Protons and neutrons were assigned random positions on the lattice sites. This procedure appeared to be better than assigning protons to alternate lattice sites since:

(i) It could be applied to neutron excess nuclei like ^{197}Au without a special algorithm for avoiding a buildup of Coulomb potential energy associated with the alternating lattice.

(ii) For some mass numbers, the alternating lattice gave rise to alternating sheets of protons and neutrons with a large associated potential energy arising from the isospin dependent interaction term.

3. The lattice structure contained a significant potential energy which resulted in an increase in the average kinetic energy of $\sim 10–12$ MeV after only a small elapsed time. Hence, the initial kinetic energy assigned to the nucleons had to be kept very low or the nuclei would be unbound. For the mass 40 and 108 systems reported here, each nucleon was randomly assigned a momentum within a sphere of radius 50 fm/c.

4. Even though the average nucleus produced by this procedure had approximately the correct rms radius, binding energy, and phase space occupancy, etc., there were some initial configurations (where many of the protons were assigned to small regions of coordinate space) which were unstable. Since we do not wish to use a configuration which ultimately fissions, the following procedure for selecting among them was adopted:

(i) a number (400 for mass 40, 100 for mass 108) of configurations were propagated for 85 fm/c using the methods outlined in subsection B.

(ii) Those initializations which were found to be unstable (about half were stable, the rest lost one or two nucleons) were discarded. The remainder were propagated for 7.5–15 fm/c and stopped at a randomly chosen time step. The sequence in which the configuration was chosen was random so that the random stopping (plus the initial assignment of random small momenta) could be used to generate a long sequence of initializations.

(iii) All initializations were then rotated arbitrarily about their center of mass.

(iv) For events where impact parameter averaging was required, the impact parameter was chosen randomly as well.

This initialization procedure is fairly time consuming. Because one of the questions of interest here is the energy dependence of reactions, the initializations for a particular projectile/target combination were stored and used at several bombarding energies.

B. Propagation

Once the initialization is complete, the nucleons are propagated classically subject to the effects of the density dependent nuclear potential and the Coulomb potential. The form taken for the mean field is

$$U(\rho) = A \left[\frac{\rho}{\rho_0} \right] + B \left[\frac{\rho}{\rho_0} \right]^2 + C\epsilon_i \left[\frac{\rho_p - \rho_n}{\rho_0} \right] , \quad (1)$$

where $\epsilon_i = +1$ (-1) for protons (neutrons). The third term represents an isospin dependent NN interaction which prevents all the protons from migrating to the nuclear surface. The value chosen for C is 25 MeV, based on optical model analysis of $p + A$ scattering.[14] The values chosen for the other two constants are $A = -124$, $B = 70.5$ MeV for both the mass 40 nucleus ($Z = 20, N = 20$) and the mass 108 system ($Z = 47$, $N = 61$).

In evaluating the Coulomb potential, it was assumed that the charge of the individual protons was uniformly distributed throughout a sphere of rms radius equal to 0.8 fm. This avoided the numerical difficulties associated with particles propagating (in a finite time step) close to the potential singularity of point charges.

For scattering, the NN cross sections are used to define an area such that if the distance of closest approach along the trajectories of two nucleons is within this area in a given time step, a collision occurs, subject to Pauli blocking. For the cross sections, we choose:

$$\sigma_{pp} = \sigma_{nn} = 22 \text{mb}, \quad \sigma_{pn} = 34 \text{ mb} . \quad (2)$$

Half of the pn scatterings result in charge exchange. The cross sections are assumed to be isotropic in the center of mass frame. The cross sections chosen are the asymptotic ones in the 200–300 MeV range. Below 100 MeV bombarding energy, the cross sections rise like p^{-2} due to the attractiveness of the long range part of the NN force. However, this attraction is as least partially accounted for here by the presence of the attractive nuclear mean field. Hence, only the asymptotic values of the cross sections are used. Pion production is not included in this code.

To evaluate the density in coordinate space [to determine $U(\rho)$] and in phase space (to determine whether a collision is Pauli blocked), the position and momentum of each nucleon are spread out by Δr and Δp around their classically assigned values according to a Gaussian:

$$e^{-\alpha^2 (\Delta r)^2} e^{-(\Delta p)^2 / (\hbar \alpha)^2} .$$

Test particles are not used here to represent this spreading

as they slow down the running of the code considerably. Instead, the density is calculated directly. For example, if we wish to find the phase space density at a particular $(\mathbf{r}_i, \mathbf{p}_i)$, to see if a collision is allowed, then the contribution of every nucleon l ($l \neq i$) to that point arising from smearing the phase space is summed over by simply evaluating the Gaussian. A comparison with the free particle phase space density then determines the phase space occupancy $f(\mathbf{r}_i, \mathbf{p}_i)$. To actually determine whether a collision is allowed, a random number is then drawn and compared with

$$[1 - f(\mathbf{r}_i, \mathbf{p}_i)][1 - f(\mathbf{r}_j, \mathbf{p}_j)]$$

for the (i,j) pair of nucleons involved in the collision. The value of α was fixed by demanding that a cold uncompressed nucleus has an average value of f as close to unity as possible. This was satisfied by $\alpha = \frac{1}{2}$ fm^{-1}.

A small modification of the proton density of states was required in determining $f(\mathbf{r}, \mathbf{p})$ to reproduce known nuclear properties. The Woods-Saxon radius parameter R has been found to be fairly similar for both proton and neutron distributions for nuclei in the mass range of interest here. If one uses these radii to predict average kinetic energies, etc., for actual values of Z and N assuming an ideal Fermi gas density of states, then the proton states turn out to have too high an energy because of the Coulomb interaction. Since it is obviously beyond the level of sophistication of this model to try to include explicitly the level densities associated with particular bound states, our method of handling this problem is to modify the free particle density of states for protons to read

$$dn(\mathbf{p}) = \frac{g\gamma}{2\pi^2} p^2 dp , \quad (3)$$

where g is the spin degeneracy factor. A value of $\gamma = 1.3$ was found to lower the proton Fermi momentum sufficiently to make the initializations stable against β decay, so to speak. Since the only place where the density of states factor enters the code is in the Pauli blocking routine, its effect on free particle propagation is negligible.

Our main objective in this paper is to use a semiclassical model to simulate the production of fragments in proton- and heavy-ion-induced reactions, at least at the qualitative level. This requires the running of a considerable number of events for each reaction, since the experimental quantities are impact parameter averaged. With a time step of 0.5 fm/c, an event with 300 time steps (long enough to allow fragments to separate out) required about 3 CPU min on an IBM 3081 for $A = 40 + A = 40$ systems and about 6 CPU min for $A = 1 + A = 108$. At this speed, accumulations of a thousand events per reaction are feasible. The choice of time step (0.5 fm/c) was chosen by comparing the mass distributions obtained for single nuclei at finite excitation energy. Changing the time step to 0.2 fm/c did not change the mass distributions by more than 10%, which was the statistical accuracy of the tests. In the same tests, energy was conserved at the level of 1 MeV per nucleon over 150 fm/c. For the problems under investigation here, namely the rapid breakup of nuclei, the accuracy carried is sufficient. This would not be the case if one wished to investigate evaporative emission on a

longer time scale. However, the more serious problem for long time scale problems is imperfect Pauli blocking.

C. Analysis

By running a reaction event for 150 fm/c, most reaction products (except some low energy evaporation products) have separated out from each other in coordinate space. Hence, the method used for determining the masses, momenta, etc. of the fragments was a simple minimum separation method. All nucleons which are separated by a distance of less than 3.0 fm are linked together to form clusters. The momentum of the cluster is, of course, determined by summing the momenta of the constituent nucleons.

III. SINGLE NUCLEI AND PROTON-INDUCED REACTIONS

The initialization procedure was tested on three nuclei to be used in these and other simulations: ^{40}Ca, ^{108}Ag, and ^{197}Au. In all three cases, the procedure produced a fairly "cold" nucleus which lost very few nucleons over the time frame of interest to these reactions. For example, the heaviest nucleus considered, ^{197}Au, typically lost less than three nucleons over 75 fm/c. This nucleus was a particularly critical test because of the large charge and neutron excess: Both of these factors decrease the binding energy per nucleon considerably compared to what is found for ^{40}Ca.

The typical behavior of the rms radius and kinetic energy per nucleon is illustrated in Fig. 1 for the ^{108}Ag initializations. The results shown are an average of five initializations. One can see from Fig. 1(a) that the rms radius is similar to that obtained from the Woods-Saxon parametrization of the density. Over long time frames the rms radius of the system begins to increase corresponding to neutron evaporation, but the increase is very slow. Figure 1(b) shows how rapidly the potential energy of the lattice is transformed into kinetic energy. Naturally, the kinetic energy is less than one would expect for an ideal square well potential nucleus because the fluctuations present in the potential here lessens the average potential well depth.

Having shown the properties of cold nuclei, let us turn now to proton-induced reactions. In a previous, somewhat simpler calculation,[15] a p + (A = 100) reaction at intermediate energies was studied. In that calculation, the potential well in which the nucleons moved was fixed externally, rather than being self-generated as in the semiclassical model. The calculation showed that very few nucleons were ejected during the transit of the projectile. In this calculation we find much the same conclusion. Shown in Fig. 2 are the (Z,N) scatter plots for the p + (A = 108) reaction at several bombarding energies. The average event (in an impact parameter average) showed very little fragmentation, so only central events will be shown. Fifty central collisions each were generated at 100, 200, and 300 MeV bombarding energy. The figure shows only those nuclei which are produced in the events, and does not show their relative frequency. However, it is clear from the fact that the reaction products are closely clustered around the maximum binding energy
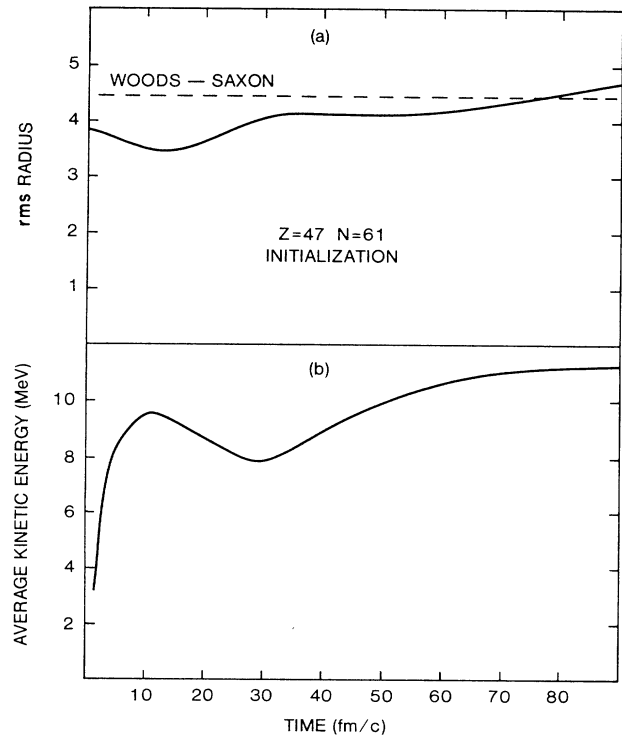

FIG. 1. Time evolution of the rms radius (a) and average kinetic energy (b) for the ^{108}Ag system used in the initialization. An average has been made over five events. The rms radius for a Woods-Saxon distribution is shown for comparison.
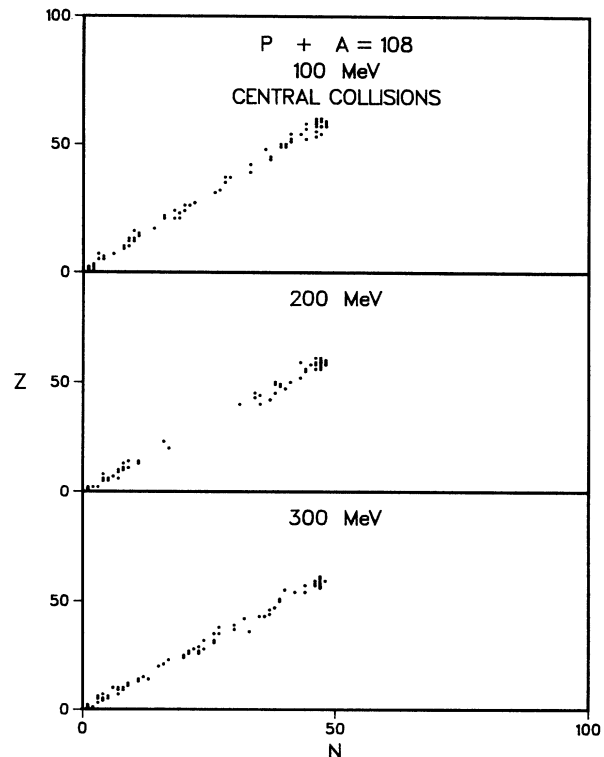

FIG. 2. Scatter plots for the reaction products found in p + (A = 108) collisions. Fifty central collisions each were used at 100, 200, and 300 MeV. The figure does not show the frequency of production of each nuclear product.

that the excitation energy of the breakup system is small (compared with the heavy ion reaction scatter plots in Sec. IV). The mass yield curves show that target breakup increases with energy, as is observed experimentally.[16] Clearly, to get any reasonable statistics on light fragment production in proton-induced reactions at these energies would require the running of perhaps 10 000 events on a random impact parameter basis. This translates into about 1000 CPU h on an IBM 3081. One could try to avoid this by running mainly central collisions, which give more fragments, and then use a weighting scheme to generate a cross section. Either method is time consuming compared to the larger fragment yields found in heavy ion collisions, and it is to them that we will now turn.

IV. HEAVY ION REACTIONS

The reaction we chose to investigate is the collision of two $(Z = N = 20)$ nuclei. Three energies were chosen: $50A$ MeV, $100A$ Mev, and $200A$ MeV in the laboratory frame. One thousand events, at random impact parameter, are generated for $100A$ MeV collisions, which will be the reaction investigated in greatest detail. For the other reactions, only 200 events will be used. Some general features of the reactions are discussed first, and then some specific comparisons with experiment are made.

Shown in Fig. 3 is a scatter plot of the reaction products for 200 events at each energy. At the lowest energy one sees a substantial amount of fragmentation, along with a few events corresponding to few particle transfer.
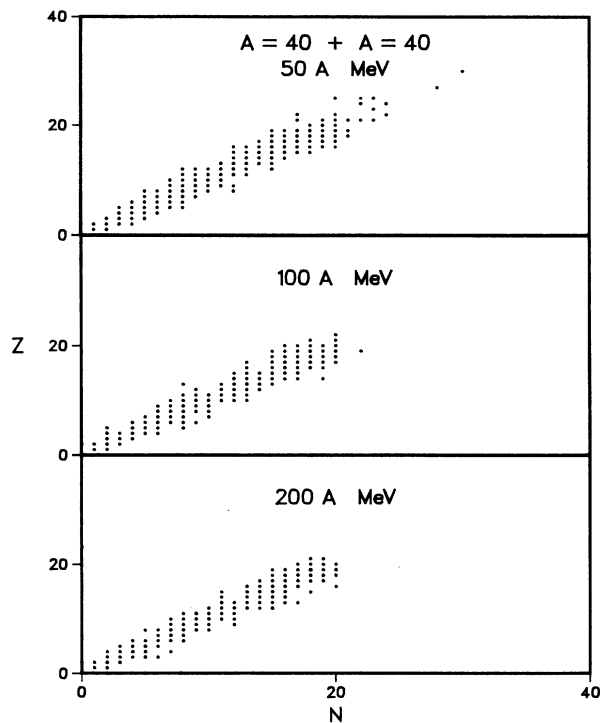
As the energy is raised to $100A$ MeV, the transfer reactions are much less frequent. Finally, at the highest energies, the reactions mainly involve particle emission from the nuclei.

One expects the degree of fragmentation to depend on the impact parameter of the reaction, and this is illustrated in Fig. 4 for the $100A$ MeV reaction. Three ranges of impact parameter were chosen: 0—3, 3—6, and 6—9 fm. The smallest impact parameters show the most violent collisions, as one would expect, while the largest impact parameters show the least amount of fragmentation.

Figures 2 and 3 show only which nuclei are produced, not their relative frequency of production. Since we have not run enough events to show the isotopic yields at the three bombarding energies, we will use mass yield curves to illustrate general features of the reactions. The isotopic yields for the $100A$ MeV reaction will be given later.

First, the mass yields as a function of A are shown in Fig. 5. At small masses, the yield falls fairly steeply and then flattens out. Often, experimental data are plotted versus the logarithm of A in an effort to represent the data as having the power law dependence $A^{-\delta}$. Such a plot is shown in Fig. 6 for fragments up to mass 15, taking the $100A$ MeV reaction as an example. One can see that a power law fit can be made over limited ranges of A. In the example shown, δ is in the range of 1.5—2.5 for light mass fragments, then decreases for heavier fragments. This is in the range of what is observed experimentally.[17] Currently, we do not have enough events to show the dependence of δ on impact parameter.

FIG. 3. Scatter plots for the reaction products found in equal mass $(Z = N = 20)$ collisions. Two hundred events were generated at each energy. Three bombarding energies are shown: 50, 100, and $200A$ MeV.
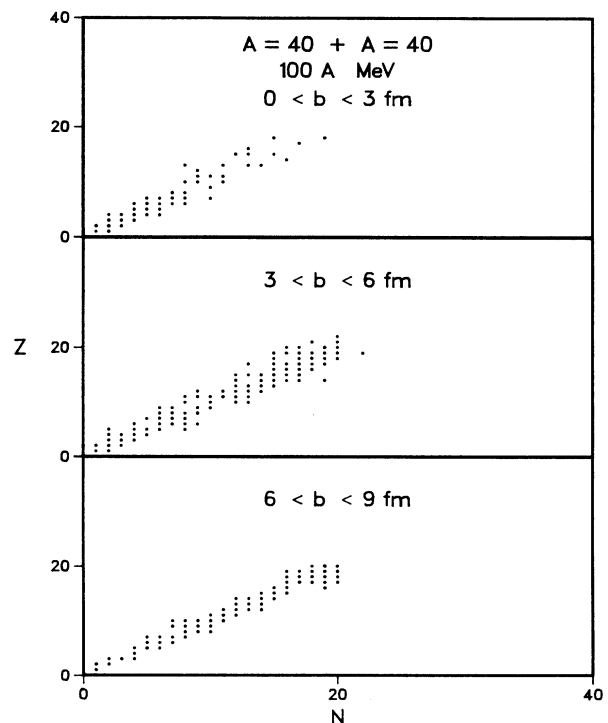

FIG. 4. Scatter plots for the reaction products found in equal mass $(Z = N = 20)$ collisions at $100A$ MeV. Three ranges of impact parameter are shown: 0—3, 3—6, and 6—9 fm.
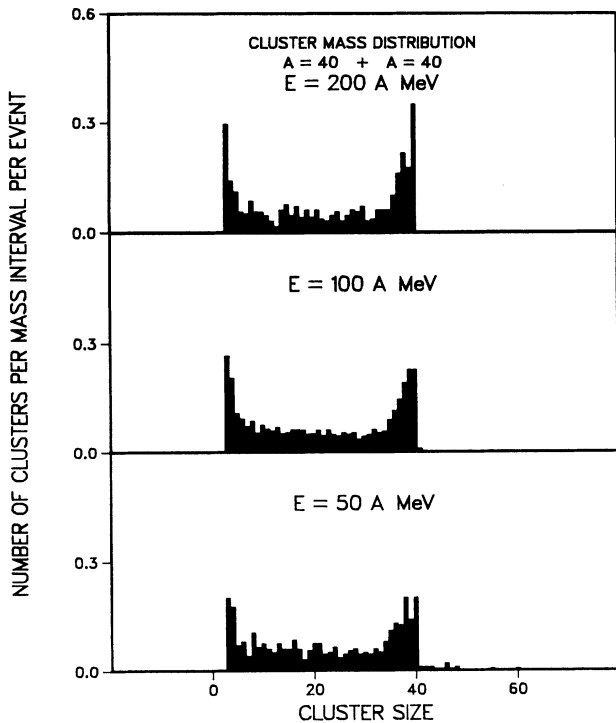
FIG. 5. Mass yield curves for $(A = 40) + (A = 40)$ at $50A$ MeV, $100A$ MeV, and $200A$ MeV bombarding energies. The yields of nucleons and deuterons have been omitted as they are off the scale of the figure.
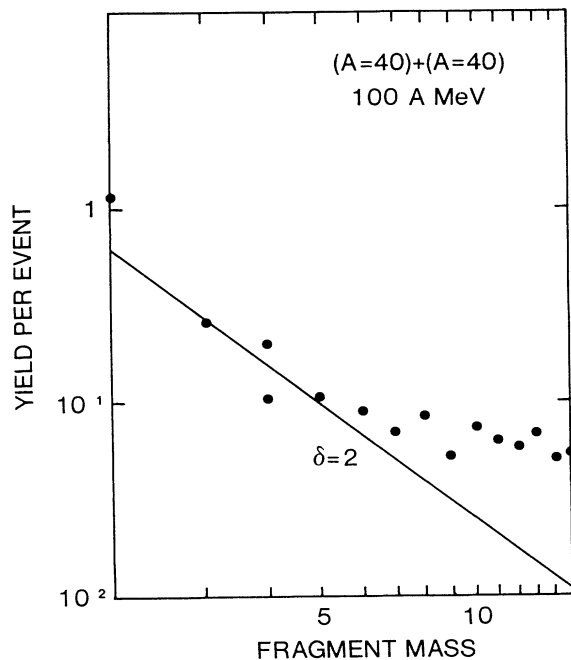

FIG. 6. Mass yields plotted as a function of the logarithm of the mass. The straight line represents $A^{-\delta}$, with the value of δ equal to 2. The reaction shown is $(A = 40) + (A = 40)$ at $100A$ MeV.

For a comparison with experimental data, the calculations at $100A$ MeV are contrasted with data[7,18] taken for the Ar + Ca reaction at $92A$ MeV. The energy integrated angular distribution of protons for these reactions is shown in Fig. 7. The normalization error for the data is not shown. The semiclassical model predictions are shown by the histogram, and appear to follow the trend of the data well. However, the predictions lie somewhat below the data. Given the additional normalization uncertainty on the data (see Ref. 18 for a discussion), it is not clear whether the discrepancy should cause concern. The proton energy spectra similarly lie below the data, although the statistics of the prediction are fairly poor. Rather than show the energy spectra, we use a method of data analysis often used in the thermal model description of reactions: At constant invariant cross section, the perpendicular component of velocity is plotted versus the rapidity along the beam axis. Such plots should be isotropic around the emitting regions at nonrelativistic energies. Shown in Fig. 8 are scatter plots for several mass numbers in the $A = 40$ equal mass collision at $100A$ MeV. The top portion of the figure is for protons and neutrons, and shows considerable evidence for multiple scattering. The bottom portion is for mass 35, where it is expected that most of the nuclei will be concentrated at the target and beam rapidities. The middle portion with $A = 4$ represents an intermediate case. All of these observations are in at least qualitative agreement with experiment.

The yields of very light fragments are not amenable to comparison in this approach. The mean field and density spreading produce an effective interaction which is only crudely comparable to the real nuclear binding present in very light fragments. However, as the mass of the fragment increases, so should the reliability of the prediction, as the mean field increasingly resembles the real nuclear potential. Shown in Fig. 9 is the yield per event (impact
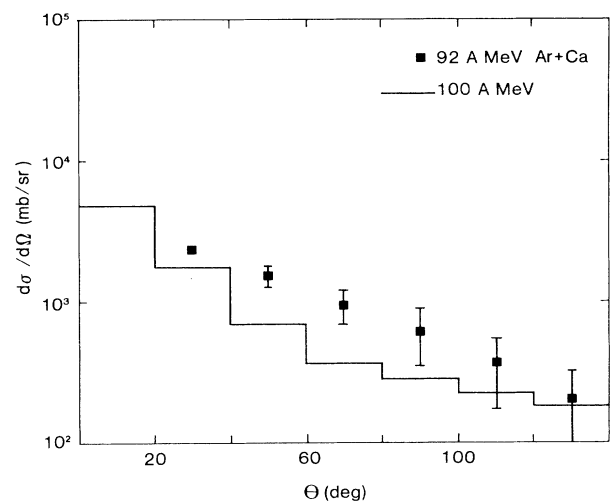

FIG. 7. Energy integrated angular distribution of protons in the Ar + Ca reaction (Ref. 16) at $92A$ MeV. Shown for comparison are the semiclassical model predictions at $100A$ MeV for the reaction of two $(Z = N = 20)$ nuclei.
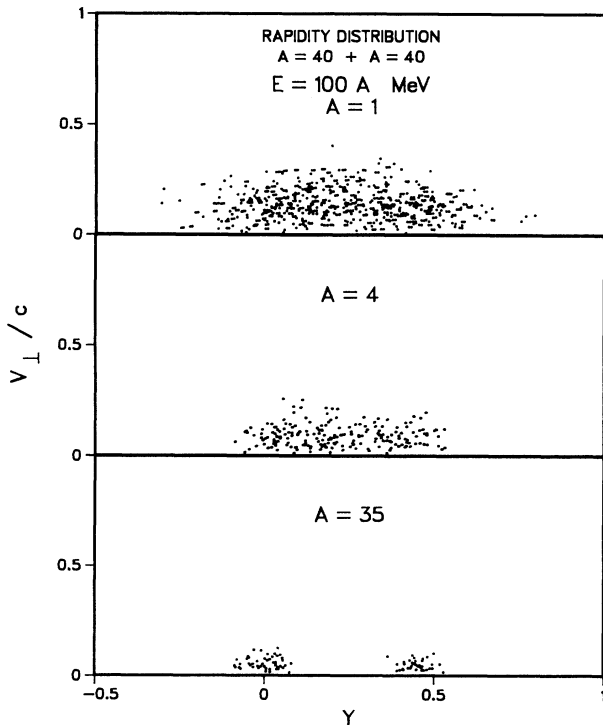
FIG. 8. Distribution of perpendicular velocity and rapidity of reaction products for $A = 1$, $A = 4$, and $A = 35$ predicted for the equal mass ($Z = N = 20$) reaction at $100A$ MeV.

parameter averaged) of light and some medium mass nuclei. The isotopic yields have a maximum for the most deeply bound nuclei, as one would expect, and then fall rapidly as one moves away from the $Z = N$ line. In addition, neutron-rich isotopes are produced in somewhat greater abundance than neutron-deficient ones. The absolute magnitude of the yields is in rough agreement with experiment, although specific comparisons cannot be made because of limited statistics.

In summary, the SCEOM model can be used to make parameter-free predictions which can be compared with heavy ion reaction data. Even discounting the normaliza-
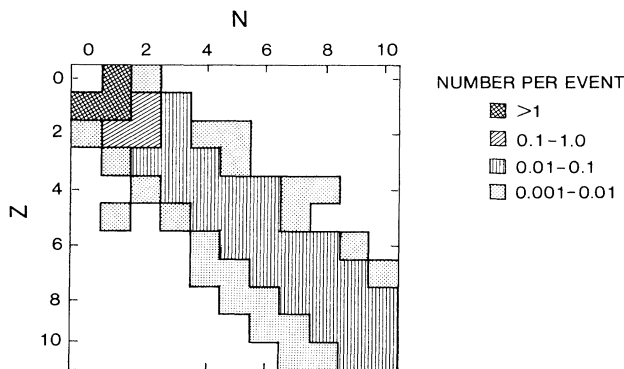

FIG. 9. Isotopic yields per event of light to medium mass fragments for ($A = 40$)+($A = 40$) at $100A$ MeV.

tion uncertainty of the data and limited statistics of the simulation, agreement is generally found at the factor of 2 level.

V. NUCLEAR INTERFEROMETRY

The use of two-particle correlations between protons[19] and between light nuclei[20,21] has allowed the extraction of some of the spatial characteristics of the reaction region, and may even allow the temperature-density reaction trajectory to be investigated.[22,23] In the analysis, a two-particle correlation function at a relative momentum Δp is obtained from the coincidence cross section for observing particles with momentum p_1 and p_2:

$$1 + R(\Delta p) \equiv \sigma_0 \frac{d^6\sigma/d^3p_1 d^3p_2}{(d^3\sigma/d^3p_1)(d^3\sigma/d^3p_2)} , \qquad (4)$$

where σ_0 is a normalization constant.

The same technique can be applied to the SCEOM events.[24] First, we search the data event by event to generate a distribution of coincidences in Δp. Then, all of the events are combined and at least ten times as many "random" coincidences are generated by randomly selecting two protons from the summed events (i.e., the events are mixed). After appropriate scaling, the true coincidences are divided by the random coincidences to generate a correlation function. This method avoids the problem of binning the single and coincident events into discrete momentum bins at an intermediate stage of the analysis. An example of the correlation function so obtained is shown in Fig. 10. As one would expect, comparatively few events are obtained at small Δp, and so the statistical uncertainties are greatest there.

A prescription advanced by Koonin[19] has often been used in the analysis of these correlation functions. The protons are assumed to be emitted from a source of Gaussian shape in space with parameter r_0 characterizing
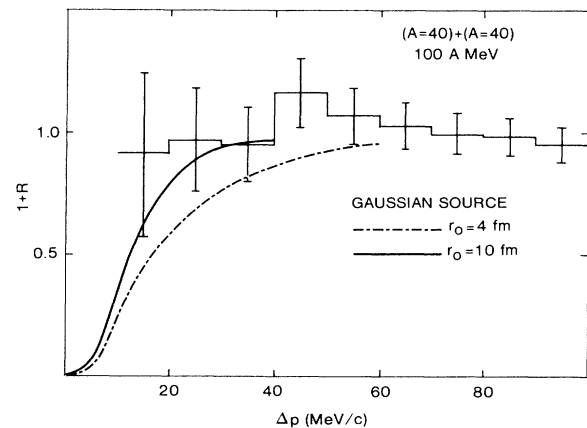

FIG. 10. Histogram shows the correlation function found from the analysis of 1000 events for the ($A = 40$)+($A = 40$) reaction at $100A$ MeV. The smooth curves are the predicted correlation functions associated with a Gaussian source (with $r_0 = 4$ and 10 fm) and wave functions generated using the nuclear mean field.

its radius (it will be assumed here that the emission of all particles occurs simultaneously). The mutual interaction of the protons causes the correlation, which can be related to their relative wave function ψ via

$$1 + R(p_1,p_2) = (2\pi r_0^2)^{-3/2} \int d^3r \exp(-r^2/2r_0^2)$$

$$\times \left\{ \tfrac{1}{4} \mid {}^1\psi_{\Delta p}(\mathbf{r}) \mid^2 \right.$$

$$\left. + \tfrac{3}{4} \mid {}^3\psi_{\Delta p}(\mathbf{r}) \mid^2 \right\} . \qquad (5)$$

The superscripts 1 and 3 refer to the degeneracy of the two proton spin states. The experimental correlation functions agree with that predicted by Eq. (5) for r_0 usually in the 3—4 fm region (depending on the reaction) and ψ generated by numerically integrating Schrödinger's equation using a Reid soft core potential. One would not expect the SCEOM correlation function to look like what is found experimentally, however, since the nucleon-nucleon interaction is governed by the mean field in the SCEOM model, not the Reid potential. To allow a comparison, then, we have used Eq. (5) to generate correlation functions with a wave function generated from the mean field. [This is somewhat brazen: The singlet potential is just replaced by Eq. (1)]. The results are shown in Fig. 10 for two choices of r_0: 4 and 10 fm.

The correlation function clearly favors larger values of r_0. This is not surprising since all protons have been summed over in generating the correlation function, including low energy ones which are quasi-evaporative in origin. We tried putting a cut on the minimum energy of the protons, but the resulting statistics were very poor. At this time, then, we are unable to draw any quantitative conclusion except that the source region for the entire proton spectrum appears to be large. To make progress on this question, far more events will be needed than the thousand used here. In addition, it may be more fruitful to pursue the molecular dynamcis approach where the Reid potential could be used directly.

VI. LIQUID-GAS PHASE TRANSITION

A considerable amount of work has gone into finding an acceptable signature for experimentally observing the liquid-gas phase transition predicted for infinite nuclear matter.[25] The observables usually involve the measurement of an inclusive quantity, often the mass distribution. For example, the power law falloff for the mass distribution has been invoked[17] as a phase transition signature. Such a power law is evident in Fig. 6, and we will see shortly whether it has to do with a phase transition. Similarly, using the yields to extract an entropy has shown[26] the puzzling behavior of the light fragments appearing to come from systems with larger entropy per nucleon than the heavier ones (target remnants are left out of these estimates). It has been suggested that this puzzle might have its origin in a liquid vapor separation.[27]

However, such observables by their very nature sum over many potentially very different reaction trajectories present in a reaction due to impact parameter averaging. The first question we wish to address with our simulation is whether these mass distributions have an impact parameter dependence. The answer appears to be yes.

Shown in Fig. 11 is the average impact parameter for each mass, summed over five mass bins in the figure. As one can see, protons and very light fragments come from larger impact parameter collisions than do medium mass fragments. As one would expect, target and projectilelike products also come from larger impact parameter collisions. These results are displayed in more detail in Fig. 12. Here the fraction of products which came from an event with a given impact parameter are shown for the $(A = 40) + (A = 40)$ reaction at $100A$ MeV. Again, the mass 35 products are strongly peripheral in origin, while mass 4's are more evenly distributed.

The main thing to be learned is that there is considerable danger in assuming that all of the reaction products can be lumped together and analyzed as having come from a common source. Here, the entropy puzzle may originate from the fact that light fragments are produced in more peripheral collisions than are intermediate mass fragments. Since there are more peripheral collisions than central ones, the yields of light fragments will be enhanced relative to medium mass ones, and the light fragments will yield an apparently higher entropy per nucleon. Of course, it could be that even after correcting for this effect, the entropy discrepancy still remains.

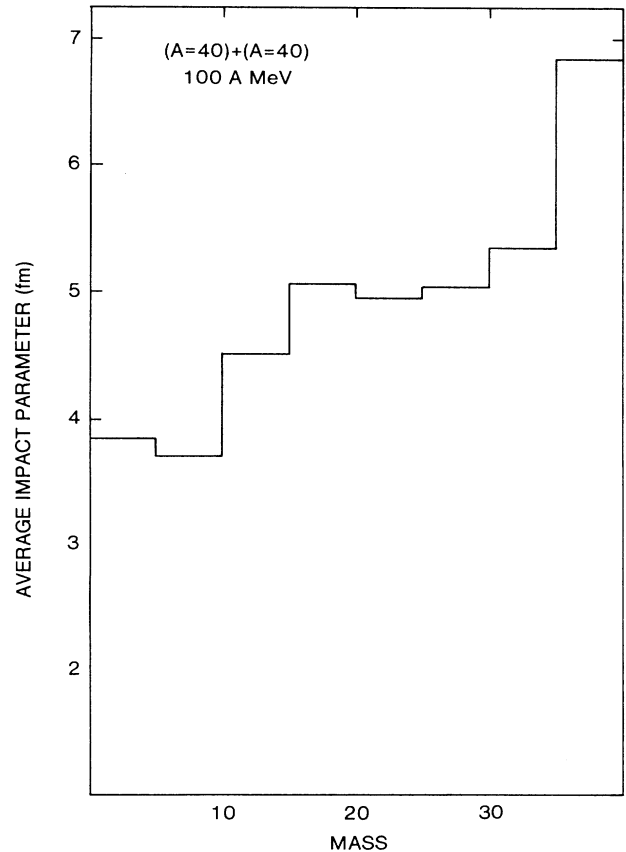The above discussion does not rule out the possibility

FIG. 11. Average impact parameter associated with a given fragment mass. The results have been averaged over five mass units for each bin. The reaction is $(A = 40) + (A = 40)$ at $100A$ MeV.
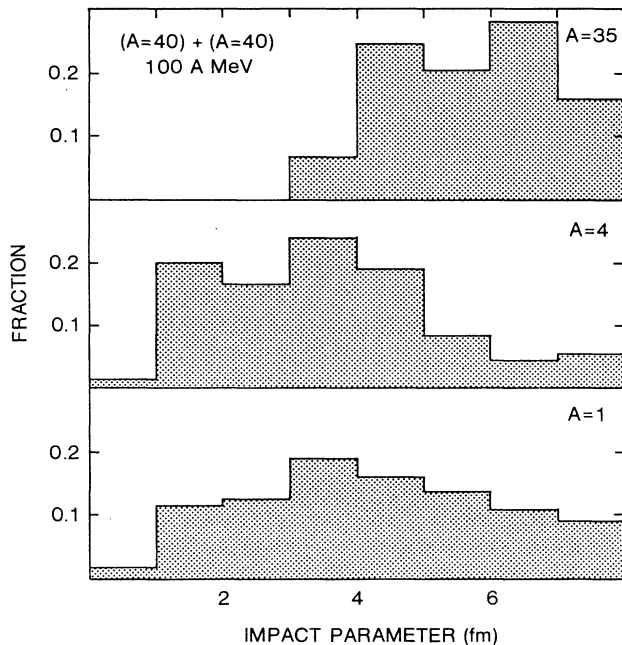
FIG. 12. Distribution of impact parameters for several different fragment masses. All results are for the $(A = 40) + (A = 40)$ reaction at $100A$ MeV.
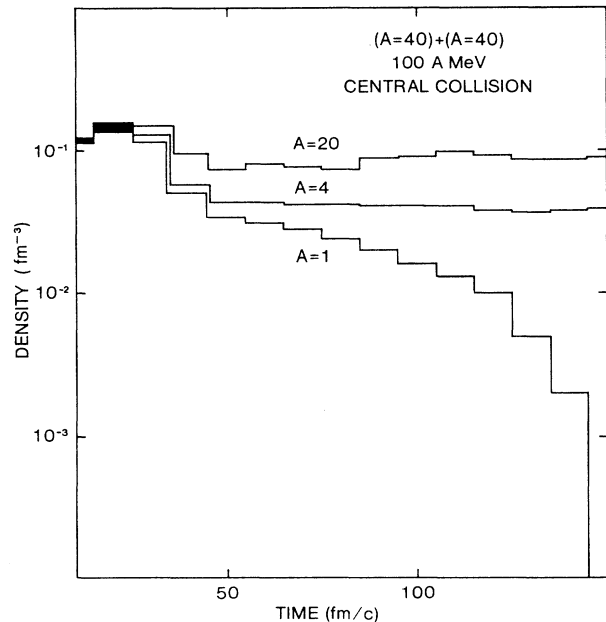

FIG. 13. Average coordinate space density for several cluster masses $(A = 1,4,20)$ shown as a function of time for a central collision of two $(a = 40)$ nuclei at $100A$ MeV.

that a liquid-vapor phase transition takes place, it only indicates that one must be careful with the signature. To investigate the phase separation question further, a sample of 100 events at zero impact parameter was generated for the $(A = 40) + (A = 40)$ reaction at $100A$ MeV. The phase space evolution of each nucleon was followed in time. At the end of the event, a cluster search routine was run to find which nucleons ended up in which cluster, so that the phase space evolution of the nucleons associated with a given cluster mass could be determined. Some of the results are shown in Figs. 13 and 14.

In Fig. 13, the average coordinate space density associated with each nucleon in a given fragment is shown for several product masses. At a time of 20 fm/c, one can see that the average density associated with all products is fairly high: The projectile and target strongly overlap. Looking at the mass 20 systems for a moment, one can see that their density decreases, then returns to the asymptotic value of ~ 0.1 fm^{-3}, with some periodic oscillation. In this sample, their average density did not drop below 0.06 fm^{-3}. However, there were regions in the reaction volume even at $t = 40$ fm/c, where the density was below 0.06 fm^{-3}, and one can see that light fragments and nucleons originate from these regions. Thus, while we cannot delineate the boundary precisely with these statistics, we see that there may be evidence for the onset of the mechanical instability region:[28] If the average density drops below a certain point the system cannot recover but breaks apart instead.

However, what we do not observe is the entire system expanding uniformly and then breaking apart at some transition density. Rather, there are already substantial
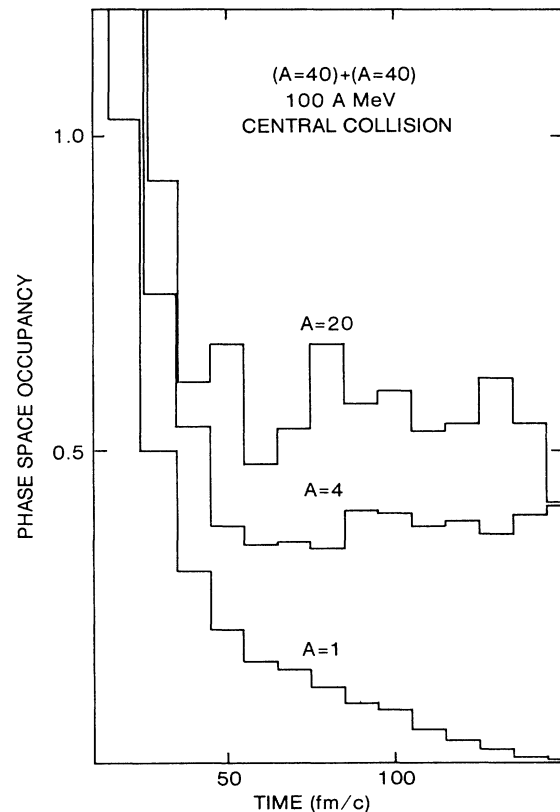

FIG. 14. Average phase space occupancy for the same conditions as Fig. 13.

fluctuations present even at early times, and these play a large role in the breakup phase. This is shown in Fig. 14, where the average phase space occupancy is shown as a function of time. Again, looking at the $A = 20$ clusters first, their average phase space occupancy oscillates around 0.6. Heavier fragments with a lower surface to volume ratio than Ne show on occupancy near unity, as one would expect. However, at $t = 30$ fm/c, there are great differences in the local phase space occupied by the light fragments, even though Fig. 13 shows their coordinate space densities to be fairly similar. One can see that nucleons that ultimately emerged as free particles ($A = 1$) have already been scattered into a low density region of phase space early in the collision. Hence, it it these fluctuations which determine the outcome of the reaction region.

VII. SUMMARY

We have formulated a semiclassical model for propagating the phase space fluctuations which develop during an energetic nuclear reaction. The interaction between nucleons is governed by an isospin dependent mean field and the Coulomb repulsion between charges where applicable. The method has been applied to several problems. First, intermediate energy p + ($A = 108$) reactions were examined. Fragmentation turned out to be relatively infrequent, although it did increase with energy as is observed experimentally. For heavy ion reactions, the second application, fragment production is much more copious, and enough events could be generated to allow experimental comparison. Some sample mass yields and angular distributions of protons were shown to agree with experiment at the factor of 2 level or better. As a function of bombarding energy, it was found that few nucleon transfer reactions decreased in importance as the bombarding energy was increased. Similarly, as a function of impact parameter, fragment production was shown to be most important for central collisions, as one would expect. In addition,

plots were made of the distribution of perpendicular velocity versus rapidity along the beam axis. These plots showed that light fragments were spread over a considerable region in velocity space, whereas heavy residual nuclei were largely clustered around the projectile and target velocities, as expected.

A two-particle correlation function was constructed from the SCEOM heavy ion events at $100\,A$ MeV. While the correlation function could not be compared directly with data, an internal comparison was made using wave functions generated with the mean field. The SCEOM correlation function was found to correspond to emission from a Gaussian source of radius parameter greater than 10 fm.

Finally, the reaction trajectories in coordinate and phase space were followed for a central collision at $100\,A$ MeV. It was found that the average density in those regions which ultimately emerged as very large fragments did not drop below about 0.06 fm^{-3} during their evolution. In the simulations, only light fragments were found to emerge from regions with lower density. However, it was also shown that phase space fluctuations generated during the collision played a crucial role in determining the extent of cluster formation. Particles which ultimately emerged as free nucleons were scattered into a low phase space occupancy region very early on in the reaction.

ACKNOWLEDGMENTS

[1]J. Cugnon, Nucl. Phys. A387, 191c (1982).

[2]H. Stocker, R. Y. Cusson, J. A. Maruhn, and W. Greiner, Z. Phys. A 294, 125 (1980).

[3]A. A. Amsden, G. F. Bertsch, F. H. Harlow, and J. R. Nix, Phys. Rev. Lett. 35, 905 (1975).

[4]A. R. Bodmer and C. N. Panos, Phys. Rev. C 15, 1342 (1977).

[5]L. Wilets, E. M. Henley, M. Kraft, and A. D. Mackellar, Nucl. Phys. A282, 341 (1977).

[6]G. Bertsch, H. Kruse, and S. Das Gupta, Phys. Rev. C 29, 673 (1984).

[7]H. Kruse *et al.*, Phys. Rev. C 31, 1770 (1985).

[8]J. Aichelin and G. Bertsch, Phys. Rev. C 31, 1730 (1985).

[9]J. J. Molitoris and H. Stocker, Phys. Rev. C 32, 346 (1985).

[10]B. Strack and J. Knoll, Z. Phys. A 315, 249 (1984); J. Knoll and B. Strack, Phys. Lett. 149B, 45 (1984).

[11]A. Vincentini, G. Jacucci, and V. R. Pandharipande, Phys. Rev. C 31, 1783 (1985).

[12]C. Gale and S. Das Gupta, Phys. Lett. 162B, 35 (1985).

[13]B. Remaud, F. Sebille, C. Gregoire, L. Vinet, and Y. Raffray, Nucl. Phys. A447, 555c (1985).

[14]I. E. McCarthy, *Introduction to Nuclear Theory* (Wiley, New York, 1968).

[15]D. H. Boal and A. L. Goodman, Phys. Rev. C 33, 1690 (1986).

[16]R. E. L. Green, R. G. Korteling, and K. P. Jackson, Phys. Rev. C 29, 1806 (1984).

[17]See, for example, references quoted in A. D. Panagioutou *et al.*, Phys. Rev. Lett. 52, 496 (1984) and D. H. Boal, Phys. Rev. C 30, 119 (1984).

[18]B. V. Jacak, Ph.D. thesis, Michigan State University, 1984.

[19]S. E. Koonin, Phys. Lett. 70B, 43 (1977).

[20]C. B. Chitwood *et al.*, Phys. Rev. Lett. 54, 302 (1985).

[21]D. H. Boal and J. C. Shillcock, Phys. Rev. C 33, 549 (1986).

[22]B. K. Jennings, D. H. Boal, and J. C. Shillcock, Phys. Rev. C 33, 1303 (1986).

[23]C. B. Chitwood *et al.*, Phys. Lett. **172B**, 27 (1986).

[24]A different method has been used to predict pion correlations. See T. J. Humanic, Phys. Rev. C **34**, 191 (1986).

[25]For refernces to previous work, see Ref. 15 as well as L. P. Csernai and J. I. Kapusta, University of Minnesota Report UMTNP-114/1985, 1985.

[26]B. V. Jacak, H. Stöcker, and G. D. Westfall, Phys. Rev. C **29**, 1744 (1984).

[27]L. P. Csernai, Phys. Rev. Lett. **54**, 639 (1985).

[28]G. Bertsch and P. J. Siemens, Phys. Lett. **126B**, 9 (1983).